CISLUNAR SPACE TRAFFIC MANAGEMENT: SURVEILLANCE THROUGH EARTH-MOON RESONANCE ORBITS

C. Frueh[(1)], K. Howell[(1)], K. J. DeMars[(2)], S. Bhadauria[(1)], and M. Gupta[(1)]

[(1)] *School of Aeronautics and Astronautics, Purdue University, 701 W. Stadium Avenue, Lafayette, IN 47907 USA, Email: {cfrueh, howell, sbhadaur, gupta208}@purdue.edu*

[(2)] *Department of Aerospace Engineering, Texas A&M University, College Station, TX 77843 USA, Email: demars@tamu.edu*

ABSTRACT

Space Traffic Management (STM) and Space Situational Awareness (SSA) are actively researched and applied in the near-Earth region. However, space fairing, including armed forces and commercial interests, is expanding into the Cislunar region, creating a need for STM and SSA in the Cislunar realm. In this paper, actual steps towards comprehensive Cislunar SSA (CSSA) are shown with the aim of establishing surveillance of the entire Cislunar region. For this aim, the suitability of the Earth-Moon 2:1 resonant orbits are investigated. This orbit family allows constructing periodic orbits covering the entire Cislunar region in just under 20 revolutions. Using ground-based sensors, the orbit can be covered with observations. A lunar ground-based sensor adds little benefits. The uncertainty propagation and orbit determination show that the 2:1 resonance orbits are very suitable for such a constellation, offering better orbit properties than many other classical orbits in the Cislunar region.

Keywords: Space Situational Awareness, Space Traffic Management, Cislunar.

1. INTRODUCTION

Cislunar space denotes the region of space between the Earth and the Moon, including the vicinity of the Earth and the Moon itself. Space Traffic Management (STM) aims at engineering solutions, methods, and protocols that allow regulating space fairing in a manner that at the same time provides access but also enables sustainable use of space. It is closely connected to Space Situational Awareness (SSA) or sometimes also called Space Domain Awareness (SDA), which aims to provide comprehensive knowledge on all objects in a specific region without necessarily having direct communication to those objects.

STM and SSA are actively researched and applied in the near-Earth region. However, space fairing, including armed forces and commercial interests, is expanding into the Cislunar region [25; 15; 1]. While at the moment, only a handful of human-made objects are in the Cislunar space further from the Earth than the geosynchronous orbital (GEO) region, this situation is about to change.

This requires the gauging of the space to begin with [22] and the finding of new metrics [8]. One focus is navigation, using GPS-like constellations [19] and other concepts [27], but also the on-orbit navigation [14]. The coverage of various orbits has been a focus [16; 9; 4; 3; 10] with ground-based or space-based sensors in terms of orbit coverage or also orbit determination [13], and orbit propagation [2]. One problem has been that not much focus has been laid on orbit construction, or in other words, that either the orbit of the gateway [4] or other popular orbits have been used [16; 9; 3; 10; 13; 14; 8]. However, such an approach is more or less random, as even the number of currently known and popular orbits is extensive. Even when only comparing to the different missions and their profiles, and as such only a small selection of orbits and parameter spaces can ever be covered. An extensive parameter search is simply not possible. On the other hand, this also leaves gaps of exact regions of space to employ a mission in case one seeks to hide.

As such, this paper is based on the previous work of the authors [10], which investigated a Lyapunov orbit, a distant retrograde orbit, and a transfer orbit. However, in this paper, the focus is shifted in order to avoid selecting random orbits with the aim of seeking to establish a methodology for complete surveillance of the entire Cislunar region. This paper presents the first steps of the investigation into the suitability of orbits and desirable properties for a space-based optical sensor carrying satellite constellation for complete Cislunar surveillance. In the following sections, the orbit

construction is discussed, followed by the investigation of the ground-based (Earth and Moon-based) coverage of the selected orbit for orbit maintenance. Subsequently, the uncertainty profile and orbit determination for orbit maintenance of the selected orbit are discussed.

2. ORBIT CONSTRUCTION

2.1. Circular Restricted Three Body Problem, Coordinate Frames, and Propagation Models

In the Earth-Moon regime, leveraging the gravity of both the Earth and the Moon offers an increase in fidelity beyond the conics. However, it can also deliver options that are phased appropriately to take advantage of the Moon to yield repeatable, predictable geometries. Thus, the Circular Restricted Three-Body Problem (CR3BP) model is useful for preliminary analysis of trajectories in this Earth-Moon system. The motion of a spacecraft is then governed by both the Earth and the Moon gravity simultaneously. To derive the mathematical model, the Earth and the Moon are defined as the primaries P_1 (mass m_1) and P_2 (mass m_2), respectively. The primaries are assumed to move on circular orbits relative to the system barycenter (BA). The barycentric rotating frame, R, is defined such that the rotating x-axis is directed from the Earth to the Moon, the z-axis is parallel to the direction of the orbital angular momentum of the primary system, and the y-axis completes the orthonormal triad. For the motion of the spacecraft in this system, the state vector is defined as $\boldsymbol{x} = [x, y, z, \dot{x}, \dot{y}, \dot{z}]^T$, which describes the spacecraft position and velocity relative to the Earth-Moon barycenter in terms of the rotating coordinates. By convention, quantities in the CR3BP are non-dimensional such that (i) the characteristic length is the distance between the Earth and the Moon; (ii) the characteristic mass is the sum $m_1 + m_2$; and, (iii) the characteristic time is determined such that the non-dimensional gravitational constant is equal to unity. The mass parameter is then defined as $\mu = \frac{m_2}{m_1+m_2}$. The first order non-dimensional equation of motion is derived in vector form as follows:

$$\dot{\boldsymbol{x}} = \boldsymbol{f}(\boldsymbol{x}), \tag{1}$$

with the vector field

$$\boldsymbol{f}(\boldsymbol{x}) = [\dot{x}, \dot{y}, \dot{z}, 2n\dot{y} + U_x, -2n\dot{x} + U_y, U_z]^T, \tag{2}$$

where n denotes the non-dimensional mean motion of the primary system. The vector field is expressed in terms of the pseudo-potential function:

$$U(x, y, z, n) = \frac{1-u}{d} + \frac{\mu}{r} + \frac{1}{2}n^2(x^2 + y^2), \tag{3}$$

where the non-dimensional quantities d and r denote the Earth-spacecraft and Moon-spacecraft distances, respectively. The quantities U_x, U_y, and U_z represent the partial derivatives of the pseudo-potential function with respect to the rotating position coordinates. The differential equation allows only a single integral of motion, termed the Jacobi constant, C, evaluated as:

$$C = 2U - v^2 \text{ with } v = \sqrt{\dot{x}^2 + \dot{y}^2 + \dot{z}^2} \tag{4}$$

The differential equations are written in terms of the rotating frame. Thus, the Jacobi constant is applicable in the rotating frame. This integral of the motion offers useful information concerning the energy level associated with a periodic orbit or a trajectory arc in the CR3BP.

Once trajectories are computed, it is frequently convenient to view them from a variety of other perspectives. For visual interpretation and clarity, views of the trajectories in the inertial frame are often insightful. A transformation from rotating to inertial coordinates is easily accomplished. An inertial frame, I, with the coordinate directions denoted by $\hat{X}, \hat{Y}, \hat{Z}$ and the rotating frame R are related such that the angular velocity of the rotating frame relative to the inertial frame is $\omega := n\hat{z} = n\hat{Z}$. Under the assumption of the CR3BP, the mean motion n is constant and is expressed as $n = \dot{\theta}$, with the angular velocity $\dot{\theta}$. Given the non-dimensional value $n = 1$, the angle θ ranges from 0 to 2π over each revolution of the Earth-Moon system in the inertial frame. The inertial frame is defined as the J2000.0 reference frame in its classical form centered on the Earth. For applications that also lean on relative behavior, e.g., the relative motion of two vehicles on nearby orbits in the circular restricted problem. The isochronous difference between the two spacecraft positions is accomplished in terms of either the rotating or inertial coordinates.

In the course of this paper, the orbits are presented under the assumptions of the CR3BP, with the point masses of the Earth and the Moon are taken into account, and the *full ephemerides model*, the Earth gravitational potential, including the main harmonic terms of (2,0) (2,2) (3,0) (3,1) (4,0) and the point gravitational sources of the Sun, the Moon and Jupiter, and Solar Radiation Pressure (SRP) have been taken into account. For the Jupiter's, lunar, and solar position, precise SPICE ephemerides are used. The solar radiation pressure model is a cannonball model with a one-meter diameter with a diffuse reflection coefficient of 0.5 and an area-to-mass ratio of 0.02 m^2/kg.

3. ORBIT CONSTRUCTION PROCESS

The Cislunar region is a harbor of many, very diverse orbits. In contrast to classical SSA applications, the

orbit construction is an integral piece. In this paper, in contrast to the authors' earlier paper [10], rather than a set of arbitrary orbits, a specific orbit is constructed and investigated to meet pre-determined criteria. The orbit is designed to connect the near-Earth region with the near-lunar region. It is an orbit for surveillance, ranging between the Earth (particularly GEO) and the Moon in one revolution and covering the entire Cislunar region in approximately 20 revolutions. A first step of expansion from the orbit is introduced, designing a constellation that is able to survey the entire Cislunar space at all times, once completed.

3.1. Earth-Moon Resonant Orbits

An important orbit of interest for the analysis of SSA applications in Cislunar space is any repeatable pathways between Earth and Moon. Resonant orbits, by their inherent definition, are periodic orbits. Resonant orbits have a long history for mission design applications with more recent consideration in the Earth-Moon system [24; 31; 28]. Resonant orbits are most straightforwardly defined in a two-body model such that a spacecraft that is orbiting Earth is in resonance with the lunar orbit. In the two-body model, the resonance is then described in terms of the relationship between the periods. If the orbital periods of the spacecraft and the Moon relative to the Earth are defined as P_{sc} and P_{moon}, then the ratio is expressed as:

$$\frac{p}{q} = \frac{P_{\text{sc}}}{P_{\text{moon}}} \tag{5}$$

For a resonant orbit, $\frac{p}{q}$ is an integer ratio. The integer p represents the number of revolutions completed by the spacecraft around the Earth, and q is equal to the number of revolutions of the Moon in the same time interval. The spacecraft is then in a $p:q$ resonance with the Moon.

Resonant orbits can be stable or unstable. Various mission design strategies leverage the unstable resonant orbits for transfer scenarios [31]. In contrast, stable orbits, particularly in the Earth-Moon neighborhood, have been successfully applied to current missions. The Interstellar Boundary Explorer (IBEX), originally launched in 2008 into a highly elliptical orbit centered at the Earth; was later transferred into a spatial 3:1 resonant orbit that guarantees long-term stability [6]. Another recent example is the Transiting Exoplanet Survey Satellite (TESS). After the spacecraft launch in 2018, TESS entered into an operationally stable spatial 2:1 resonant orbit [7]. A sample trajectory that exploits resonant orbits, as well as their distinctive repeating geometry, is useful to examine sensitivities in Cislunar space.

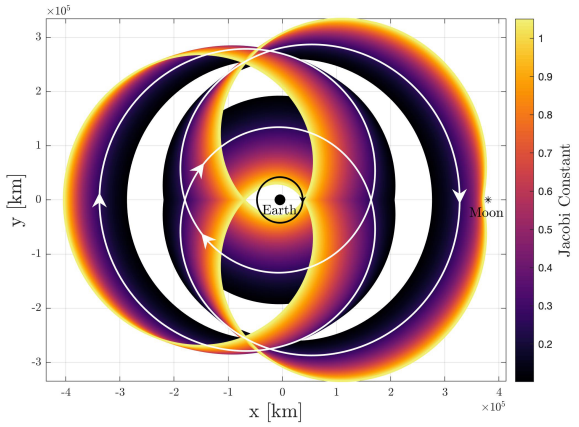

(a) In Rotating Frame R

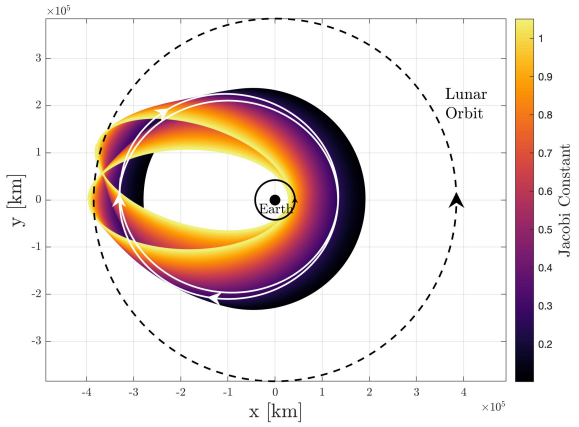

(b) In Inertial Frame I

Figure 1: Family of 2:1 Resonate Orbits in the Circular Restricted Three Body Problem.

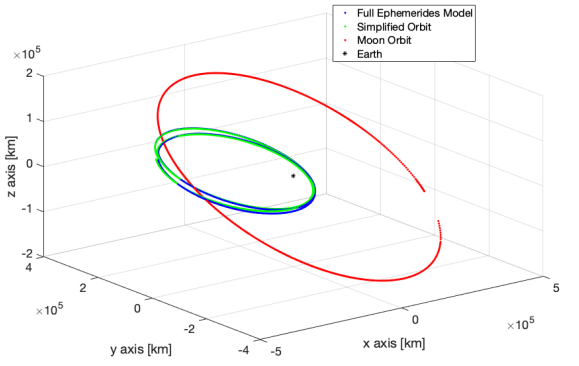

Figure 2: Selected resonance orbit propagated with the two different dynamical models, simplified CR3BP dynamics and full ephemerides models in the inertial J2000.0 frame.

Resonant ratios identified in the two-body problem are frequently transitioned to the CR3BP since the additional fidelity offers additional options. The resonant orbits exist as isolated orbits in the two-body problem. However, in the CR3BP, the resonant orbits expand to families of solutions. Incorporating the additional gravity field and the autonomous nature of the CR3BP allows families of resonant planar as well as spatial orbits to exist. The resulting orbits do not possess a perfect integer ratio of periods relative to the orbit of the Moon in the Earth-Moon system. Thus, the spacecraft completes p revolutions of the Earth in *approximately* the same time that the Moon complete q revolutions about the Earth. In addition, the transitioned orbit is no longer precisely periodic. However, a differential correction process produces a family of precisely periodic orbits. Thus, a family of orbits offers periodicity and a range of periods and energy levels throughout the family. Such a family of orbits can subsequently be transitioned to a higher-fidelity ephemerides model.

For the analysis of the Earth-Moon region and the challenges that orbits in the Cislunar region might produce for SSA applications, some straightforward orbits are sought. A planar orbit that explores the Cislunar region between Earth and Moon offers insight into the problem. A sample family of planar resonant orbits are plotted in Fig. 1. This family of trajectories is a 2:1 resonant orbit family, i.e., each orbit requires approximately twice the Lunar orbits period to complete each revolution. Each orbit also extends throughout the region, specifically between Earth and Moon. Although not the complete family, this subset includes orbits that pass near the Earth and also in the near vicinity of the Moon.

For the further analysis, a reference orbit is selected corresponding to the Jacobi Constant (JC) of 0.8964. Fig.2 shows the comparison in the inertial J2000.0 frame between the simple dynamics model of the CR3BP and the full numerically integrated ephemerides model. It can be seen that the orbit transfers well into the realistic dynamics and retains its properties well. This is not always the case, as can be seen in [10]. The selected resonance orbit can be formed into an exact periodicity covering the entire Cislunar disc, as shown in Fig.3 about 20 revolutions in the inertial frame in the CR3BP dynamics. The orbit is diving retrograde into the geostationary (GEO) region and back to the moon at each single revolution.

An additional relevant orbital issue involves a consideration of the orbit for a potential satellite constellation of spacecrafts with on-board observation capabilities. The dynamics is not as such, that one could have a simple chaser constellation, as the periodicity with the Moon would be violated. The 2:1 resonant planar orbit is unstable as assessed via

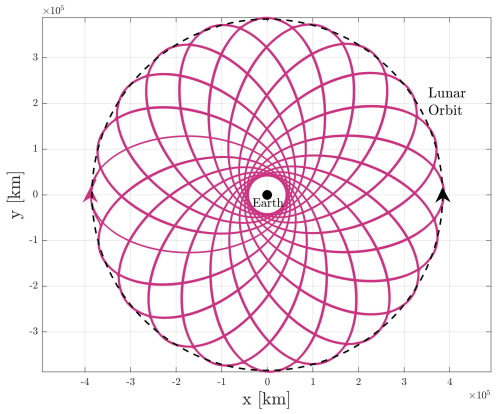

Figure 3: JC 0.8964 2:1 resonant orbit over 20 revolutions in inertial space mapping out the entire Cislunar region.

the traditional Floquet criteria for periodic orbits [33; 12]. However, the metric is so close to linearly stable that for all practical consideration the orbit is linearly stable. Using nearby orbits of the same family allows the adding of one additional deputy, which is explicitly shown in Fig.4. The deputy shall stay in a relative vicinity to the original chief satellite, without the danger of collisions. Assuming observing capabilities of covering medium sized objects optically with the on-board sensor leads to the deputy orbit selection from the same family with the JC 0.8721. Here, chief and deputy keep a distance safe for operational purposes of over 500km minimally and up to 8500km, as shown in Fig.5.

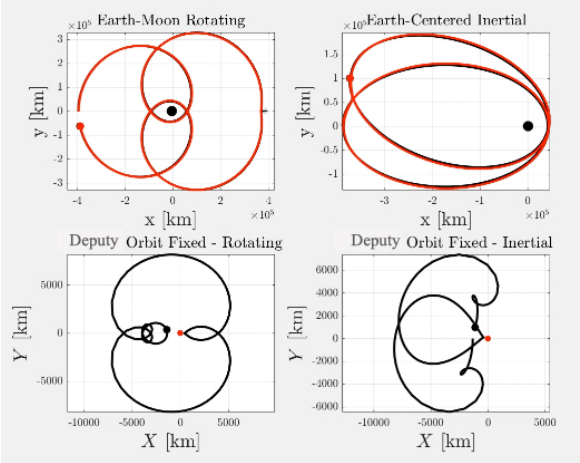

Figure 4: Overview of the chief and deputy orbital configuration of the two orbits of the 2:1 resonant family.

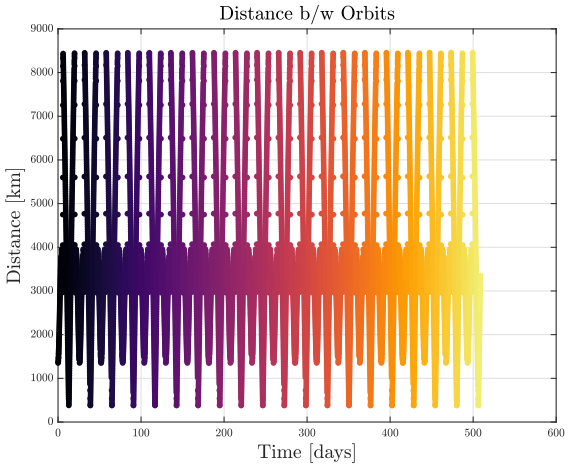

Figure 5: Distance between chief and deputy both in the 2:1 resonance orbits with JCs of 0.8964 and 0.8721, respectively.

4. SURVEILLANCE OF THE 2:1 RESONANT ORBIT

One of the key elements in Cislunar Space Surveillance is the coverage of the orbits with observations. While the on-orbit observers will provide surveillance the Cislunar region, independent ground-based observations are also needed in order to maintain the orbits of the observer constellation satellites independent of the constellation itself. In the following, the possibilities of ground-based observers on both, the Earth and the Moon are investigated.

4.1. Optical Modeling

A comprehensive treatment of optical sensor modeling can be found in [11; 26], here the relevant pieces for the problem at hand are shown. In order to model the optical sensor, the magnitude of a representative space object on the selected sample orbits is computed. The magnitude of a space object is:

$$\text{mag} = \text{mag}_{\text{sun}} - 2.5 \log_{10}(\frac{I_{\text{sc}}}{I_{\text{sun}}}) \tag{6}$$

where mag_{sun} is the apparent reference magnitude of the Sun, I_{sc} is the irradiance reflected off the spacecraft, and I_{Sun} is the Sun's reference irradiance. In order to compute the irradiance that is reflected off the object, an assumption about the albedo-area, the shape, and attitude of the space object has to be made. In this paper, a baseline case of a Lambertian sphere is chosen, which is in full agreement with the solar radiation pressure modeling. Overall, for satellites in a box-wing configuration, higher irradiation is received in the case of a specular glint off the solar panels or the antennas. However, those glints are, per definition, not continuous and only occur during limited times over one period, if at all, depending on the Sun-object-observer geometry. The irradiance of the object can be expressed via the following relation [11]:

$$sI_{\text{sc}} = \frac{I_{\text{Sun}}}{d^2_{\text{sc}_{\text{obs}}}} \frac{2}{3} \frac{C_d}{\pi^2} r^2 (\sin\alpha + (\pi - \alpha)\cos\alpha) \tag{7}$$

$d_{\text{sc}_{\text{obs}}}$ is the distance between the object and the observer, r is the object's radius, and α is the phase angle between the Sun and the observer at the object's location. It is important to note that the solar constant I_0, needs to be scaled to the actual distance between the Sun and the object $d_{\text{Sun}_{\text{sc}}}$ for the reference irradiance $I_{\text{Sun}} = I_0 \frac{\text{AU}^2}{d^2_{\text{Sun}_{\text{sc}}}}$ as the solar constant is defined at one Astronomical Unit (AU). This is relevant when computing the absolute irradiation of the object.

For the visibility besides the overall magnitude also the background irradiation entering the sensor are relevant, creating the so-called detection signal to noise ratio (SNR) in its definition is the mean divided by the standard deviation [18]:

$$\text{SNR} = \frac{S}{\sqrt{S+N}}, \tag{8}$$

S and N denote the mean (and variance) of the Poisson distributed signal of interest and the noise. In our case, the signal of interest is the signal contained in the object image on the detector, and the noise is in those same pixels.

The detection limit is directly dependent on the SNR and is dictated by the exact setup of the optic's aperture, sensor type, and sensitivity in combination with the specific image processing software. While, for methodologies employing stacking, detection limits can be pressed to be below an SNR of 1. This requires precise tracking and is inversely proportional to the time spent observing the object, which is not realistic or feasible in many cases.

Nighttime visibility constraints are often listed as a separate observation constraint; however, strictly speaking, nighttime constraints are also SNR constraints. Daytime imaging of satellites in off-Sun directions is possible; however, the higher background requires a much higher object magnitude to reach the same SNR. For this reason, night time constraints are applied, requiring observations to take place after astronomical sunset.

The observations are assumed to be ground-based, local horizon constraints for both Earth and Moon. A local horizon constraint of 0 degrees above horizon has been employed, again serving as the lowest possible limit; in realistic observations, elevations below 10 degrees are often avoided because of atmospheric attenuation effects.

4.2. Earth Ground-Based Observer

Fig. 6 shows the magnitude for the Earth ground-based observer located at about 40.4 degrees North and 86.9 degrees East, as a sample location. The observations start on Jan 1, 2020, at midnight; the orbit is propagated with the full ephemerides model for over 25.96 days. The object is assumed to be spherical with a Lambertian reflectivity of 0.9. In the plot, multiple radii are shown. It has to be noted that only the largest objects are visible at times, even for sensors that can detect up to magnitude 20. The objects are brightest at the geostationary passage. It has to be noted that in this specific instance, the sharp rise to magnitude up to 35 is not driven by the distance, as this is still part of a passage closest to the Earth, but by the phase angle geometry from the observer to the Sun. As such, one can see that considerations of distance along can be oversimplifying. One can also see that the background moonlight [23] does play a significant role and thwarts observations, especially between 200 and 300 hours, even if more sensitive telescopes would be available and the object is sufficiently large.

Fig. 7 shows the observation possibilities for a global network of ground-based sensors of a one-meter radius object with reflectivity of 0.9. 400 sensors have been distributed with a spacing of 4.7 degrees in latitude and 18.9 degrees in longitude around the Earth. The sensor spacing is illustrated on the Earth (not to scale) in Fig. 7: a sensor is placed at each grid point center. To determine, if observations are possible, the following constraints are applied: Observations are only possible during local astronomical night time and when the object appears above the local horizon (astronomical sunset/sunrise, above zero elevation), has a magnitude brighter than 20, and an SNR of larger than $\sqrt{S/2}$. The points in the orbit, which are observable, are shown in pink. The ones where none of the sensors can cover the object with observations are shown in black. In Fig. 7 , the situation at the last observation epoch at the end of the propagation period is shown, with yellow the sensors that can provide observations and blue the ones that do not have visibility. One can see that even with a global ground-based sensor network and a high limiting magnitude, large observation gaps exist.

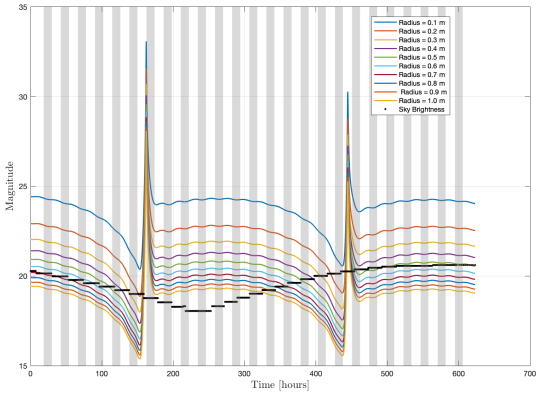

Figure 6: Earth Ground-Based Observer at 40.4 deg N, 86.9 deg E: Magnitude of a spherical object in the 2:1 resonant orbit as a function of time. Gray bars show astronomical night times, in black background sky brightness according to stay moonlight in the observation directions.

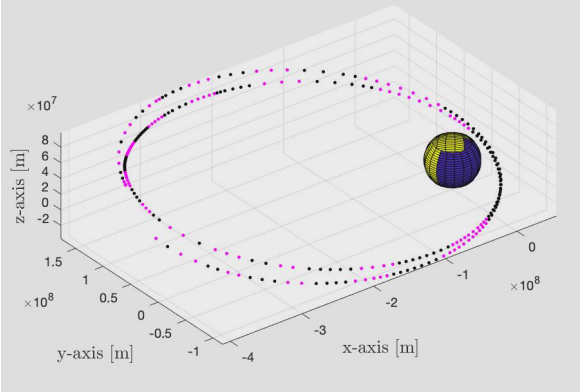

Figure 7: Trajectory of the object in Earth centered inertial frame and visibilities for Earth ground-based observers. Ground-based sensor locations with visiblities at the end time of the propagation are yellow , the ones without are marked in blue (Earth size not to scale), the trajectory, for which at least one ground-based sensor has a visibility at the time is marked pink, otherwise black.

4.3. Moon Ground-Based Observer

For Cislunar Space Situational Awareness, Moon is also explored as a location for Moon ground-based sensors. Fig.8 shows the magnitude of a Moon ground-based observer located at 50 degrees South, 150 degrees East on the lunar surface. The epoch is again the time since Jan 1, 2020, with the propagation time of 25.96 days. It can be observed that even for a telescope with a limiting magnitude 20, only two regions of good observing conditions for large objects exist. Again, those are not exactly the locations at which the objects are closest to the observer because of the phase angle.

Fig. 9 shows the situation for a global network of ground-based sensors. A sensor is assumed to be located at the center of each grid point (Moon not to scale), with 400 sensors in total. The orbit is shown in the Moon centered inertial frame. A limiting magnitude of 20 is assumed, a lunar surface elevation angle of larger than zero, and observations are only permitted between local lunar astronomical sunset and sunrise. The object is assumed to have a radius of one meter and a reflectivity of 0.9 as a spherical Lambertian reflector. The points in pink are the orbital locations for which observations are possible for at least one ground-based sensor, and in black, the regions where no observations are possible for any of the sensors under the given constraints. It can be seen that the global sensor network on the Moon does not significantly differ from the situation of the single sensor shown in Fig. 8. As such, the lunar observation base does not give, at least in this example, as great of an advantage as one would have hoped for, given the cost and effort to build a global sensor network on the Moon.

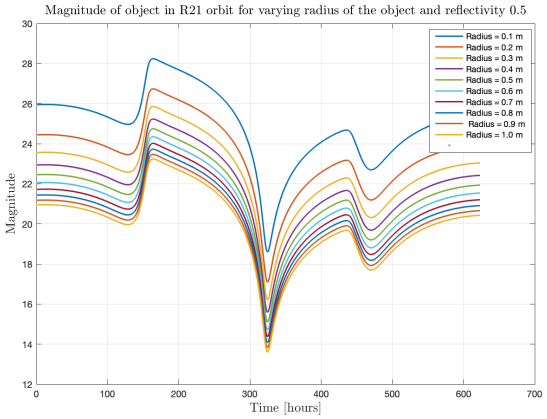

Figure 8: Moon Ground-Based Observer at 50 deg S, 150 deg E: Magnitude of a spherical object in the 2:1 resonant orbit as a function of time. Gray bars show astronomical night times, in black background sky brightness according to stay moonlight in the observation directions.

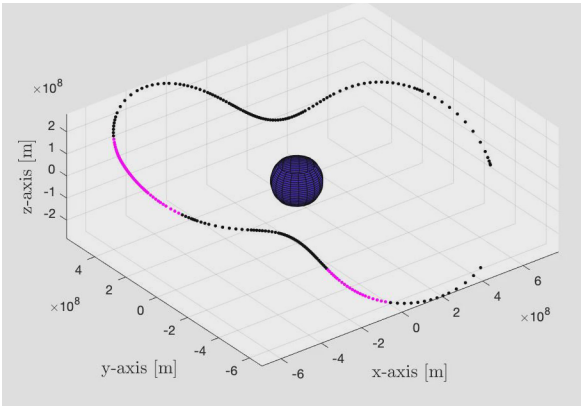

Figure 9: Trajectory in the Moon centered inertial frame of the object and visibilities for Moon ground-based observers. The trajectory, for which at least one ground-based sensor has a visibility at the time is marked pink, otherwise black. Observers are assumed at the center of each grid location on the Moon (Moon not to scale).

5. UNCERTAINTY PROPAGATION

Accurate propagation of uncertainty facilitates better awareness of the space environment. A common implementation of uncertainty propagation involves propagating central moments, i.e., mean and covariance, of the distribution using elements of the extended, unscented, or quadrature Kalman filter. These approaches have inherent limitations in their ability to represent distributions that exhibit curvature or multi-modality. Recent work has expanded upon the propagation of the central moments by introducing alternative representations of the uncertainty. The Gaussian mixture approach, pioneered in [29], for instance, has been successfully applied in a number of orbit-related applications [5; 17; 30; 32].

A Monte Carlo simulation is used to assess the influence of the Cislunar environment on the propagation of uncertainty. A set of 1000 Monte Carlo trials is carried out, where the initial position and velocity are resampled for each trial, using 1σ values of 10 m and 10 m/s are used for each channel of the position and velocity, respectively, and the sampled initial conditions are propagated for a duration of 26 days. The resulting orbits are illustrated in Fig. 10, where it is noted that the results presented here focus on relatively large initial velocity uncertainties in an effort to expose the differences in the Cislunar and near-Earth environments.

In order to investigate the distributional characteristics of the Monte Carlo samples, position dispersions away from an initially unperturbed propagation are shown in Fig. 11, and Fig. 12 shows the projections of the individual samples along with various combinations of the position coordinates after 7 days, 14 days, and 26 days of propagation time. The po-

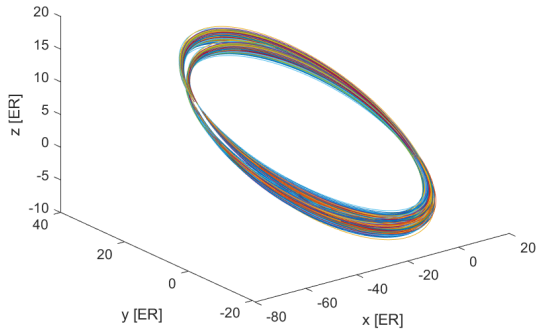

Figure 10: Propagated orbits for the full ephemerides model starting from perturbed initial conditions.

sition dispersions indicate that the propagated uncertainty cannot, after a period of time, be represented by a Gaussian distribution, as the dispersions no longer exhibit symmetry (about the horizontal direction) after a period of time. Whereas it has been found that uncertainty propagation in the Cislunar environment can produce complex structures in the uncertainty that can described as "crossovers" and "coils" [10], the results of Fig. 12 indicate that the distribution about the reference orbit considered here remains relatively well behaved, as there is only minor curvature present in the distribution. As such,

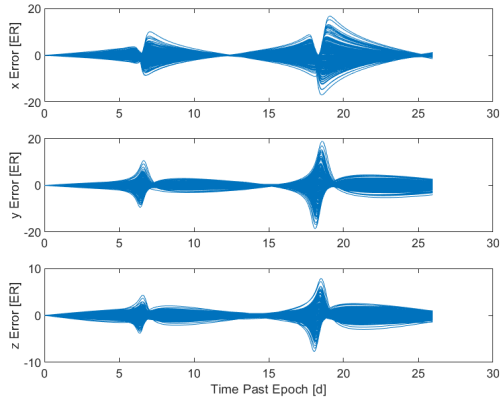

Figure 11: Position dispersions for the full ephemerides model starting from perturbed initial conditions.

the orbit is showing desirable properties, which are much more managable than the ones of other orbits in the Cislunar realm [10].

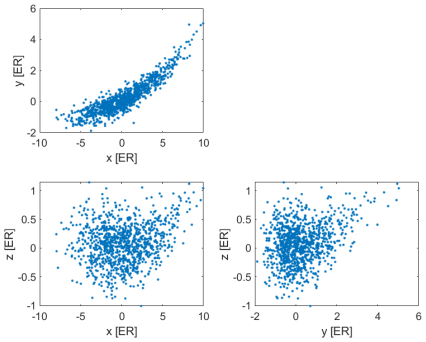

(a) After 7 Days

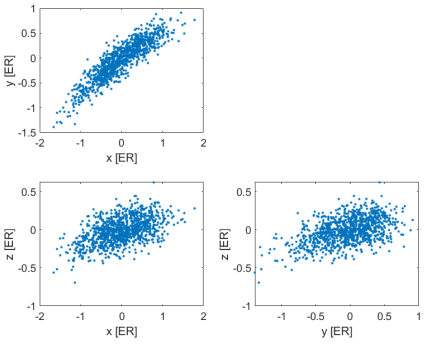

(b) After 14 Days

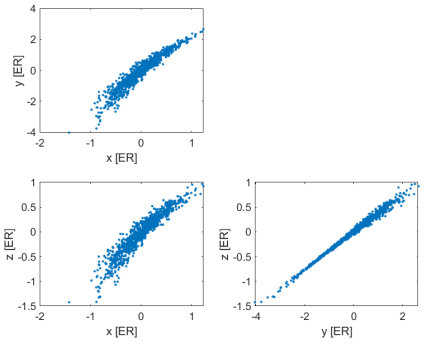

(c) After 26 Days

Figure 12: Full ephemerides model: Projections of samples onto the x-y, x-z, and y-z planes for the full ephemerides model propagation starting from perturbed initial conditions.

6. ORBIT DETERMINATION

An unscented Kalman filter (UKF) [20] is applied to process right-ascension and declination measurements taken over the course of 26 days by the network of global Earth ground-based sensors introduced in section 4.2. While this presupposes a global coverage, it assumes the sensors are employed in other activities, only taking minimal time to observe the desired orbit. Hence, in total, a set of 56 measurements of the right ascension and declination are

simulated, where the correspondence between measurement time and measurement index is illustrated in Fig. 13. From Fig. 13, it is observed that the first measurement occurs approximately 7 days following the initial time of the simulation. A sequence of 27 measurements is acquired between 7 and 9 days after the initial time. The 28^{th} measurement is not acquired for another 10 days, at which time the remaining measurements are acquired over the course of two more days. This measurement sequence leads to two large periods of time during which the UKF is required to propagate the uncertainty before processing additional data.

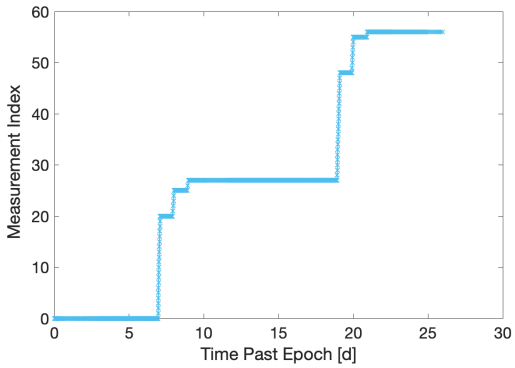

Figure 13: Relationship between measurement index and the time past epoch.

Measurements of right-ascension and declination are simulated with $3''$ (1σ) of additive, Gaussian measurement noise. The UKF is applied to the entire sequence of data in accordance with the scaled, unscented transform [21] with parameters $\alpha = 0.5$, $\kappa = 6.0$, and $\beta = 2.0$. These parameters are used in both the propagation and update stages of the UKF. The initial conditions are taken to be sampled from the nominal trajectory using a zero-mean Gaussian distribution with a diagonal covariance with standard deviations of 10 m in each position channel and 1 m/s in each velocity channel. To test the UKF, a Monte Carlo simulation consisting of 100 trials is carried out. For each trial, the initial estimated state and the measurement noise are resampled. Fig. 14 presents the state estimation errors and associated estimated filter 3σ curves for the first 20 trials, and Fig. 15 presents the measurement innovations and associated estimated filter 3σ curves for the first 20 trials. In Figs. 14 and 15, the estimation errors and measurement innovations that are plotted are shown in terms of the absolute values as the blue curves. The orange curves are the filter 3σ values. From both of these figures, it is readily observed that the UKF successfully maintains tracking of the object throughout the entire sequence of simulated data. The two larger spikes observed in every plot of Figs. 14 and 15 coincide with the large period of propagation preceding the 1^{st} and 28^{th} measurements. After the last measurement is processed, the estimated uncertainty in terms of the root-sum-square of the estimated standard deviations is 2.06 km in position and 1.51 cm/s in velocity.

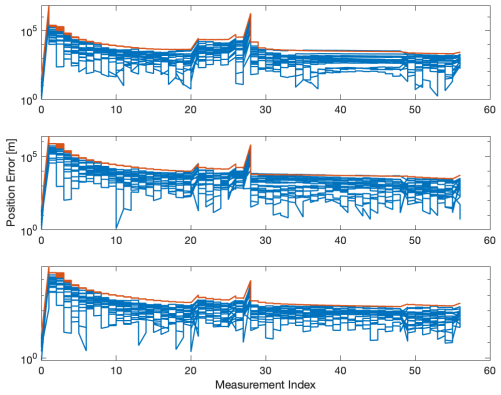

(a) Position

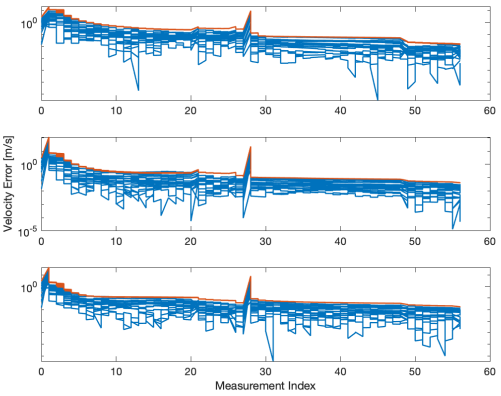

(b) Velocity

Figure 14: State estimation errors for the UKF.

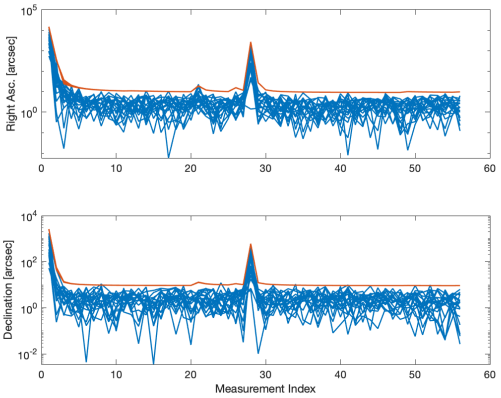

Figure 15: Measurement innovations for the UKF.

7. CONCLUSIONS

In conclusion, it was possible to construct an orbit family with many desirable properties for the surveillance of the Cislunar region.

The 2:1 resonant orbit family provides many desirable properties, connecting the near-Earth with the near-Moon region. The orbits of the family that have been selected for further consideration dive into the geostationary region in a retrograde fashion and go out to the Moon once in every period of just around 26 days. The nearly stable orbits because they are precessing under the Moon's gravitational influence provide full coverage over the entire Cislunar disc in a periodic motion of around 20 revolutions. The desired orbital characteristics are easily maintained in a high fidelity propagation of the orbit.

A chief and deputy constellation of two orbits has been proposed as a first stepping stone to show, as a proof-of-concept, the possibility to populate the region with several objects in such 2:1 resonant orbits. The two-satellite constellation shown here can successfully keep a safe distance at all times.

Independent observations for the selected orbit are possible via Earth ground-based sensors, whereas a global spread of the sensors is crucial. The lunar background light, decreasing the signal-to-noise ratio, is an important factor to consider, limiting observations. Moon ground-based sensors offer for this particular orbit only a small advantage.

The uncertainty characteristics of the orbit are extremely good and a lot more manageable compared to many other orbits in the Cislunar realm that are regularly used. This allows for the successful orbit determination and orbit maintenance using an Unscented Kalman Filter framework relying on a global spread of Earth ground-based sensors with a limiting magnitude of 20 and minimal observation time per sensor only.

The very positive results of this groundwork allow for further expansion of the concept on 2:1 resonant orbits towards the framework of a full on-orbit observer satellite constellation.

REFERENCES

1. Air Force eyeing technology to monitor space traffic near the moon, Apr. April, 2020. Website: spacenews.com.
2. Amato, D., Rosengren, A. J., and Bombardelli, C. THALASSA: a fast orbit propagator for near-Earth and cislunar space. In *2018 Space Flight Mechanics Meeting* (2018), American Institute of Aeronautics and Astronautics.
3. Banks, B., II, R. S., R.G. Wagner, V. A., Williams, S., and M.Duncan, S. De Smet, M. B. A Sensor-Rich Solution for Lunar/Cislunar Space Domain Awareness. In *Proceedings of the 2003 AMOS Technical Conference, September 2020, Maui, Hawaii, USA* (2020).
4. Bolliger, M., Thompson, M., Ré, N., and Davis, D. Ground-Based Navigation Trades for Operations in Gateway's Near Rectilinear Halo Orbit. In *31st AIAA/AAS Space Flight Mechanics Meeting* (2021).
5. DeMars, K., and Jah, M. Probabilistic initial orbit determination using radar returns. In *Proceedings of the AAS/AIAA Astrodynamics Specialist Conference Hilton Head* (2013).
6. Dichmann, D., Lebois, R., and Carrico, J. Dynamics of Orbits Near 3:1 Resonance in the Earth-Moon System. *Journal of the Astronautical Sciences 60*, 1 (2013), 51–86.
7. Dichmann, D., Parker, J., Williams, T., and Mendelsohn, C. Trajectory Design for the Transiting Exoplanet Survey Satellite. In *24th International Symposium on Space Flight Dynamics, Laurel, Maryland, May* (2014).
8. Fowler, E., Paley, D., and Hurtt, S. Observability Metrics for Space-Based Cislunar Domain Awareness. In *31st AIAA/AAS Space Flight Mechanics Meeting* (2021).
9. Fowler, E. E., Hurtt, S. B., and Paley, D. A. Orbit Design for Cislunar Space Domain Awareness. In *2nd IAA Conference on Space Situational Awareness (ICSSA), Washington, District of Columbia* (2020).
10. Frueh, C., Howell, K., DeMars, K., and Bhadauria, S. Cislunar Space Situational Awareness. In *31st AIAA/AAS Space Flight Mechanics Meeting* (2021).
11. Frueh, C., Little, B., and McGraw, J. Optical Sensor Model and its Effects on the Design of Sensor Networks and Tracking. In *Advanced Maui Optical and Space Surveillance Technologies Conference (AMOS)* (Sept. 2019).
12. Gupta, M. *Finding Order in Chaos: Resonant Orbits and Poincaré Sections.* Purdue University, West Lafayette, IN, 2020. Master Thesis.
13. Hinga, M. Spacebourne Orbit Determination of Unknown Satellites Using a Stabilized-Gauss-Method, Linear Perturbation Theory and Angle-Only Measurements. In *Proceedings of the 2003 AMOS Technical Conference, September 2018, Maui, Hawaii, USA* (2018).
14. Hinga, M. Cis-Lunar Autonomous Navigation via Implementation of Optical Asteroid Angle-Only Measurements. In *Proceedings of the 2003 AMOS Technical Conference, September 2020, Maui, Hawaii, USA* (2020).

15. Hitchens, T. US Needs New Policies With Move To Cislunar: Aerospace Corp., June, 2020. https://breakingdefense.com/2020/06/us-needs-new-policies-with-move-to-cislunar-aerospace-corp/, last accessed, 2020-07-30.

16. Holzinger, M. J., and Vendl, J. K. Cislunar periodic orbit analysis for persistent space object detection capability. In *Astrodynamics Specialist Conference, Portland, ME* (2019).

17. Horwood, J. T., Aragon, N. D., and Poore, A. B. Gaussian sum filters for space surveillance: Theory and simulations. *Journal of Guidance, Control, and Dynamics 34*, 6 (November-December 2011), 1839–1851.

18. Howell, S., Koehn, B., Bowell, E., and Hoffman, M. Detection and measurement of the poorly sampled point sources imaged with 2-D arrays. *Astronomical Journal 112 (3)* (1996), 1302 – 1311.

19. Jenner, L. NASA Eyes GPS at the Moon for Artemis Missions, June 2019. http://www.nasa.gov/feature/goddard/2019/nasa-eyes-gps-at-the-moon-for-artemis-missions, last accessed 2020-07-30.

20. Julier, S., and Uhlmann, J. Unscented filtering and nonlinear estimation. In *Proceedings of the IEEE* (March 2004), vol. 92,3.

21. Julier, S. J. The scaled unscented transformation. In *AACC American Control Conference* (2002).

22. Knister, S. *Evaluation Framework for Cislunar Space Domain Awareness (SDA) Systems.* Air Force Institute of Technonolgy, Wright Patterson AFB, Ohio, 2019. Master Thesis.

23. Krisciunas, K., and Schaefer, B. A Model of the Brightness of Moonlight. *Astronomical Society of the Pacific 103* (1991), 1033–1039.

24. Murray, C., and Dermott, S. *Solar System Dynamics.* Two Volumes. Cambridge University Press, Cambridge, United Kingdom, 1999.

25. Ruhe, J. SDA's Kennedy: Cislunar Space The Next Military Frontier, April, 2019. https://breakingdefense.com/2019/04/sdas-kennedy-cislunar-space-the-next-military-frontier/, last accessed at 2020-07-30.

26. Sanson, F., and Frueh, C. Noise Estimation and Probability of Detection in Nonresolved Images: Application to Space Object Observation. *Advances in Space Research 64*, 1432.

27. Scott, K., and Krupiarz, C. Ccsds cislunar communications architecture. In *SpaceOps 2006 Conference* (2006).

28. Short, C., Howell, K., Haapala, A., and Dichmann, D. Design of Transfer Trajectories Between Resonant Orbits in the Restricted Three-Body Problem with Application to the Earth-Moon System. *Journal of the Astronautical Sciences 64*, 2 (2017), 156–187.

29. Sorenson, H. W., and Alspach, D. L. Recursive Bayesian estimation using Gaussian sums. *Automatica 7* (1971), 465–479.

30. Terejanu, G., Singla, P., Singh, T., and Scott, P. Uncertainty propagation for nonlinear dynamic systems using Gaussian mixture models. *Journal of Guidance, Control, and Dynamics 31*, 6 (November-December 2008), 1623–1633.

31. Vaquero, M., and Howell, K. Design of Transfer Trajectories Between Resonant Orbits in the Restricted Three-Body Problem with Application to the Earth-Moon System. *Acta Astronautica 94*, 2 (2014), 302–317.

32. Vittaldev, V., Linares, R., and Russell, R. P. Spacecraft uncertainty propagation using gaussian mixture models and polynomial chaos expansions. *Journal of Guidance, Control, and Dynamics 39*, 9 (2016), 2163–2169.

33. Zimovan-Spreen, E.M., K. H., and Davis, D. Near Rectilinear Halo Orbits and Nearby Higher-Order Dynamical Structures: Orbital Stability and Resonance Properties. *Celestial Mechanics and Dynamical Astronomy 132*, 23 (2020).